

Our results demonstrate that the viscosity of aqueous fluids increases only slowly with increasing silicate content. The viscosity of a fluid with 20 wt % (12 mol %) silicate at 800°C, for example, is equal to that of pure water at room temperature (1.0×10^{-3} Pa s), and that of a fluid with 50 wt % (35 mol %) silicate at the same condition is comparable to olive oil at room temperature (0.8×10^{-1} Pa s). The low viscosity of such silicate-rich fluids, together with their favorable wetting properties compared with silica-poor fluids (21, 22), allows them to migrate out of the subducting slab even at low volume fractions and to infiltrate the overlying mantle wedge along channels or grain boundaries. High contents of dissolved silicate could be a prerequisite for the mobilization of subduction-related aqueous fluids, because silicate-poor fluids remain trapped in the slab as a result of their high wetting angles (23). Therefore, it may be no coincidence that volcanic fronts occur only at positions where complete miscibility between aqueous fluids and silicate melts is possible [~ 70 to 150 km above the subducting plate (24, 25)]. Our results also suggest that the fast ascent rates of subduction-derived material observed in certain arc lavas (26) do not necessarily indicate transport by means of a near-endmember aqueous fluid, but could be accomplished by liquids with high silica contents. The possibility of material transport by silica-rich hydrous fluids should therefore be considered in any quantitative model of element recycling in subduction zone environments.

References and Notes

1. Y. Tatsumi, S. Eggins, *Subduction Zone Magmatism* (Blackwell, Cambridge, 1995).
2. A. H. Shen, H. Keppler, *Nature* **385**, 710 (1997).
3. H. Bureau, H. Keppler, *Earth Planet. Sci. Lett.* **165**, 187 (1999).
4. R. A. Lange, in *Volatiles in Magmas*, M. R. Carroll, J. R. Holloway, Eds. (Mineralogical Society of America, Washington, DC, 1994), vol. 30, pp. 331–369.
5. W. A. Bassett, A. H. Shen, M. Buckum, *Rev. Sci. Instrum.* **64**, 2340 (1993).
6. A. H. Shen, W. A. Bassett, I. M. Chou, in *High-Pressure Research: Application to Earth and Planetary Sciences*, Y. Syono, M. H. Manghni, Eds. (American Geophysical Union, Washington, DC, 1992), pp. 61–68.
7. Materials and methods are available as supporting material on Science Online.
8. The cell was overhanging by 4° to ensure free fall of the spheres.
9. H. R. Shaw, *Am. J. Sci.* **272**, 870 (1972).
10. I. Kushiro, *Earth Planet. Sci. Lett.* **41**, 87 (1978).
11. D. B. Dingwell, in *Magmatic Processes: Physicochemical Principles*, B. O. Mysen, Ed. (The Geochemical Society, University Park, PA, 1987), pp. 423–431.
12. F. Schulze, H. Behrens, F. Holtz, J. Roux, W. Johannes, *Am. Mineral.* **81**, 1155 (1996).
13. International Association for the Properties of Water and Steam (IAPWS), revised release on the IAPWS Formulation 1985 for the viscosity of ordinary water (IAPWS, Erlangen, Germany, 1997).
14. R. P. Rapp, B. E. Watson, *J. Petrol.* **36**, 891 (1995).
15. J. Adam, T. H. Green, S. H. Sie, C. G. Ryan, *Eur. J. Mineral.* **9**, 569 (1997).

16. J. Hermann, D. H. Green, *Earth Planet. Sci. Lett.* **188**, 149 (2001).
17. G. Prouteau, B. Scaillet, M. Pichavant, R. Maury, *Nature* **410**, 197 (2001).
18. M. E. Schneider, D. H. Eggler, *Geochim. Cosmochim. Acta* **50**, 711 (1986).
19. R. C. Newton, C. E. Manning, *Geochim. Cosmochim. Acta* **66**, 4165 (2002).
20. The entire data set of the system albite-H₂O is represented by the formula

$$\log \eta = -4.2 + \left\{ m_a \left(\frac{c_{\text{solids}}(\text{wt } \%)}{100} \right)^3 + m_b \left[1 - \left(\frac{c_{\text{solids}}(\text{wt } \%)}{100} \right)^3 \right] \right\} \times \left(\frac{10,000}{T} - 2 \left[1 - e^{-\frac{c_{\text{water}}(\text{wt } \%)}{15}} \right] \right)$$

where $m_a = 1.68 - 0.42[c_{\text{water}}(\text{wt } \%)]^{0.29}$, $m_b = 0.008 c_{\text{solids}}(\text{wt } \%)$, and e is the base of the natural logarithm.

21. E. B. Watson *et al.*, in *Continental Mantle*, M. A. Menzies, Ed. (Clarendon Press, Oxford, 1990), pp. 111–125.
22. B. J. Wannamaker, D. L. Kohlstedt, *Phys. Chem. Miner.* **18**, 26 (1991).

23. S. Ono *et al.*, *Earth Planet. Sci. Lett.* **203**, 895 (2002).
24. J. Gill, *Orogenic Andesites and Plate Tectonics* (Springer, New York, 1980).
25. Y. Tatsumi, *Geophys. Res. Lett.* **17**, 717 (1986).
26. S. P. Turner, R. M. M. George, A. M. Evans, C. J. Hawkesworth, G. F. Zellmer, *Philos. Trans. R. Soc. London Ser. A* **358**, 1443 (2000).
27. C. Romano, B. Poe, V. Mincione, K. U. Hess, D. B. Dingwell, *Chem. Geol.* **174**, 115 (2001).
28. H. Scholze, *Glas—Natur, Struktur und Eigenschaften* (Springer, New York, 1988).
29. R. H. Doremus, *Glass Science* (Wiley, New York, ed. 2, 1994).
30. We thank C. Berthold, T. Wenzel, N. Walker, and B. Maier for their technical assistance, and S. Geiger (ETH Zürich) for help with H₂O viscosities. A.A. acknowledges support by an Alexander von Humboldt fellowship. This work was also financed by the German Science Foundation (D.F.G.; Leibniz award to H.K.).

Supporting Online Material

www.sciencemag.org/cgi/content/full/303/5657/513/DC1

Materials and Methods

SOM Text

References

7 October 2003; accepted 16 December 2003

Evidence That Nitric Acid Increases Relative Humidity in Low-Temperature Cirrus Clouds

R. S. Gao,^{1*} P. J. Popp,^{1,2} D. W. Fahey,^{1,2} T. P. Marcy,^{1,2} R. L. Herman,⁵ E. M. Weinstock,⁶ D. G. Baumgardner,⁸ T. J. Garrett,⁹ K. H. Rosenlof,¹ T. L. Thompson,¹ P. T. Bui,¹⁰ B. A. Ridley,¹¹ S. C. Wofsy,⁷ O. B. Toon,³ M. A. Tolbert,^{2,4} B. Kärcher,¹² Th. Peter,¹³ P. K. Hudson,^{1,2} A. J. Weinheimer,¹¹ A. J. Heymsfield¹¹

In situ measurements of the relative humidity with respect to ice (RH_i) and of nitric acid (HNO₃) were made in both natural and contrail cirrus clouds in the upper troposphere. At temperatures lower than 202 kelvin, RH_i values show a sharp increase to average values of over 130% in both cloud types. These enhanced RH_i values are attributed to the presence of a new class of HNO₃-containing ice particles (Δ -ice). We propose that surface HNO₃ molecules prevent the ice/vapor system from reaching equilibrium by a mechanism similar to that of freezing point depression by antifreeze proteins. Δ -ice represents a new link between global climate and natural and anthropogenic nitrogen oxide emissions. Including Δ -ice in climate models will alter simulated cirrus properties and the distribution of upper tropospheric water vapor.

Water (H₂O) vapor plays a critical role in Earth's climate system (1, 2) and is considered the most important greenhouse gas in the atmosphere (3–5). Cirrus clouds are a principal component of the water cycle and climate system because of their role in dehydration and their interaction with visible and infrared radiation (6–8). Cirrus cloudiness induced by persistent contrails is a principal uncertainty in determining the contribution of aviation to the radiative forcing of climate (9). Water vapor uptake on ice particle surfaces is generally assumed to control the equilibrium relative humidity with respect to ice, RH_i, in

natural and contrail cirrus clouds. The characteristic high particle number and surface area density (SAD) of persistent contrails are expected to be particularly effective in maintaining RH_i at 100% (10–12). Although the effects of chemical impurities on the nucleation of liquid and solid cloud particles are well recognized (13–15), the possibility that chemical impurities might enhance RH_i in cirrus clouds has not been proposed. Here, we show that RH_i is increased about 100% at low temperatures in natural cirrus clouds and persistent contrails in the upper troposphere and, further, we propose that the mechanism for

this increase is the formation of a new class of HNO_3 -containing ice particles.

Airborne in situ measurements in both cloud types were made at subtropical latitudes in summer 2002 (16). The derived values of RH_i are shown in Fig. 1 as a function of ambient temperature. The cloud data all were selected to have SADs greater than $100 \mu\text{m}^2 \text{cm}^{-3}$ (16). Natural cirrus cloud data from 10 July flights show an average RH_i value of 113% above 202 K and 135% below 202 K. On four of the flights, HNO_3 adsorbed on cloud particles was also measured. These data show average RH_i values above and below 202 K that are similar to the 10-flight averages. Although many previous observations show RH_i values well above 100% in and out of clouds (17–20), few in-cloud observations are available at temperatures below 210 K. Equilibrium RH_i values are expected to be 100% in a dense cirrus cloud in the absence of strong wave activity or radiative heating and cooling (21). Some previous observations show increased frequency of RH_i values above 100% with decreasing temperature (20).

Ambient RH_i is calculated from measurements of water vapor, pressure, and temperature, and from laboratory measurements of the water vapor pressure over ice (16). The aircraft payload included two water vapor measurements based on independent techniques and two similar pressure and temperature measurements (16). For all the flight data shown here, agreement between the various component measurements establishes high confidence in the precision of the RH_i determination. The average precision of the RH_i measurements is approximately $\pm 5\%$, indicating that the scatter in cirrus RH_i in Fig. 1 is primarily due to natural variability. The RH_i accuracy is $\pm 11\%$ based on an estimate of total systematic error (16). Between 202 and 230 K in Fig. 1, the average RH_i value of 113% is nearly equal to the expected value of

100% within the $\pm 11\%$ accuracy. Below 202 K in Fig. 1, the average RH_i values exceed 100% by an average of near 35%, which is much greater than the estimated 11% accuracy. This high average value in natural cirrus clouds and contrails is the focus of the discussion below.

All cirrus clouds are dynamic systems, continuously evolving as wave activity, temperature, radiation, or water vapor amounts change locally and as ice particles grow, evaporate, and undergo gravitational sedimentation. With only the limited number of observations of natural cirrus in Fig. 1, the average RH_i value of 135% at temperatures below 202 K cannot be defined confidently as an equilibrium value. However, the contrail observations of enhanced RH_i help establish this confidence. Contrail cirrus clouds differ from natural cirrus clouds because their ice particles have higher number concentrations (100 to 200cm^{-3} versus $\ll 100 \text{cm}^{-3}$) and smaller sizes (0.5 to $3 \mu\text{m}$ versus $>20 \mu\text{m}$ diameter). As a consequence, the relaxation

time for water vapor to reach an equilibrium value with the contrail ice surface typically requires less than 1 min (12). Because the contrail data in Fig. 1 are associated with contrail ages between 5 and 40 min, the associated RH_i values are considered representative of equilibrium conditions (16). Wave activity or related perturbations are not expected to increase average RH_i by more than 3% above the equilibrium value in the contrails sampled here (22). Similarly, perturbations to the equilibrium state in natural cirrus caused by gravity waves associated with convection are not considered important for data in Fig. 1 (22).

In the 13 July contrail, with temperatures between 196 and 200 K, RH_i values average 131% and show no temperature dependence. The enhanced values are consistent with the natural cirrus value of 135% below 202 K. In contrast, the 19 July contrail data show a significant temperature dependence, with RH_i increasing below 202 K. The increase of about 10% occurs over 1.2 K and a short

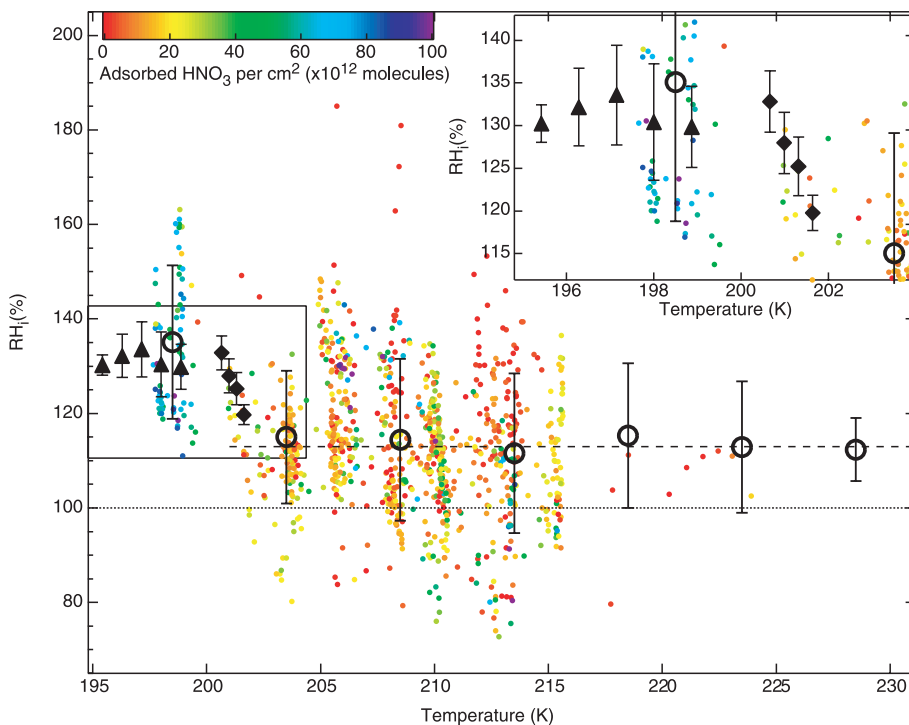


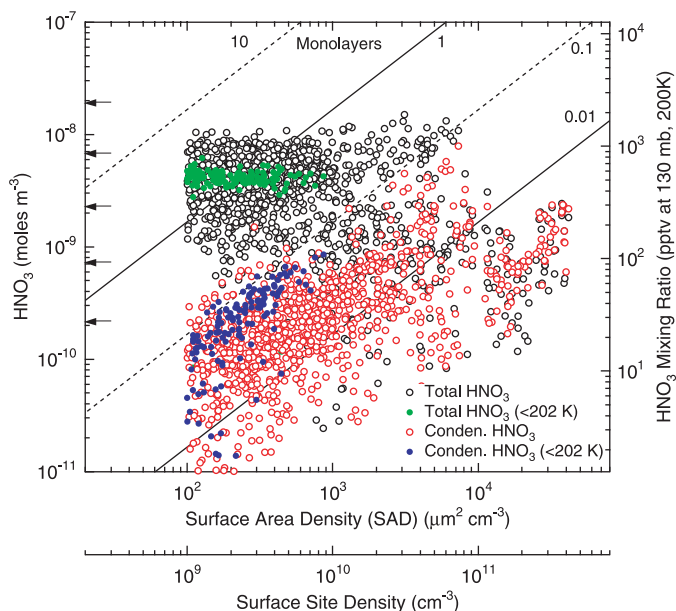
Fig. 1. RH_i values as a function of temperature for measurements obtained in cirrus and contrail clouds over southern Florida during the NASA Cirrus Regional Study of Tropical Anvils and Cirrus Layers—Florida Area Cirrus Experiment in July 2002. The open black circles are values averaged in temperature bins for the entire aircraft data set [4000 data points (each a 10-s average) taken over 10 flights]. The points are plotted at the average temperature of each bin with vertical bars that show the standard deviation in each 5 K temperature bin. The clouds were sampled at an altitude between 10 and 15 km. The horizontal dashed line at 113% represents the average of data above 202 K. The cloud data were chosen to have ice SAD greater than $100 \mu\text{m}^2 \text{cm}^{-3}$. The colored points are from four flights for which HNO_3 data are also available (11, 13, 19, and 21 July). The colors correspond to adsorbed HNO_3 surface coverage of cirrus ice as shown by the color bar. The black solid triangles and diamonds represent averages of 1-s contrail data for 13 July (270 data points) and 19 July (72 data points), respectively, over temperature bin widths of 0.86 and 0.33 K, respectively. Vertical bars on the contrail points show the standard deviation in each temperature bin. Data for temperatures less than 204 K are expanded in the inset. The contrail measurements confirm the uptake of HNO_3 on contrail particles, but the large uncertainty in the surface area measurements at small particle sizes precludes calculating a surface area coverage.

¹Aeronomy Laboratory, National Oceanic and Atmospheric Administration, Boulder, CO 80305, USA. ²Cooperative Institute for Research in Environmental Sciences; ³Laboratory for Atmospheric and Space Physics, Program in Atmospheric and Oceanic Sciences; ⁴Department of Chemistry and Biochemistry, University of Colorado, Boulder, CO 80309, USA. ⁵NASA Jet Propulsion Laboratory, Pasadena, CA 91109, USA. ⁶Atmospheric Research Project, ⁷Department of Earth and Planetary Sciences, Harvard University, Cambridge, MA 02138, USA. ⁸Universidad Nacional Autónoma de México, Centro de Ciencias de la Atmósfera, Ciudad Universitaria, 04510 México DF, México. ⁹Department of Meteorology, University of Utah, Salt Lake City, UT 84112, USA. ¹⁰NASA Ames Research Center, Moffett Field, CA 94035, USA. ¹¹Atmospheric Chemistry Division, National Center for Atmospheric Research, Boulder, CO 80307, USA. ¹²Institut für Physik der Atmosphäre, Deutsches Zentrum für Luft- und Raumfahrt, Wessling, Germany. ¹³Laboratorium für Atmosphärenphysik, ETH-Zürich, CH-8093 Zurich, Switzerland.

*To whom correspondence should be addressed. E-mail: rgao@al.noaa.gov

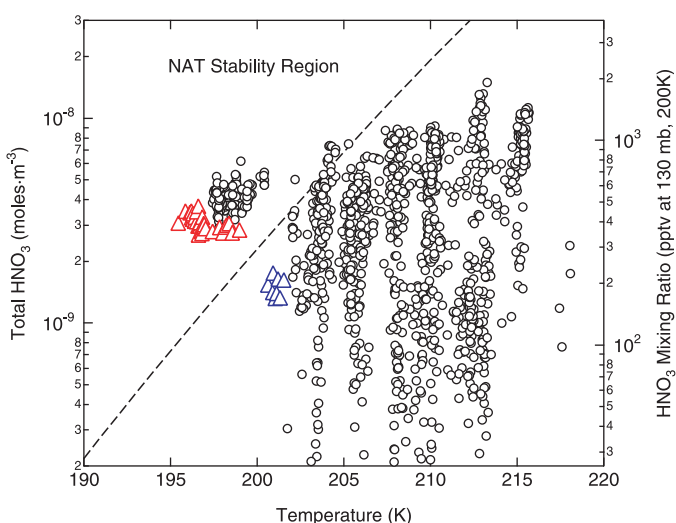
(7-min) sampling period. This dependence is particularly important because it suggests a temperature threshold for increased RH_i values. The observation of this threshold is not affected by the accuracy of the RH_i measurements and hence offers strong support for a systematic difference between RH_i above and below 202 K, independent of the natural cirrus observations.

Fig. 2. HNO_3 amounts as a function of measured SAD in natural cirrus clouds. The points are 10-s averages representing two data sets: total available HNO_3 (black points) and condensed-phase HNO_3 on ice (red points). Within each data set, the symbol type indicates ambient temperature above (open circles) and below (solid circles) 202 K. Each data set corresponds to the data set of colored points in Fig. 1. Vertical axes represent HNO_3 abundances in units of total moles m^{-3} and the equivalent gas-phase mixing ratio at 130 hPa and 200 K. The mixing ratio scale is accurate for all points



within a factor of 2 because of the limited pressure and temperature range of the measurements. The horizontal axes represent SAD and surface site concentrations, with the latter calculated using a constant value of 10^{15} sites cm^{-2} for a surface monolayer. Surface coverage of NAT will be proportionately larger than the coverage of HNO_3 alone by about a factor of 3. The diagonal lines represent constant monolayer coverage as labeled. SAD measurements by two independent techniques are in agreement, except for contrail particle data which are not shown (supporting text). The small arrows indicate the equilibrium gas-phase HNO_3 amounts on the NAT/ice phase boundary at the noted temperatures. These amounts are the minimum required for bulk NAT to be stable at the designated temperatures.

Fig. 3. Measured total HNO_3 values plotted as a function of ambient temperature in natural cirrus clouds and contrails. Total HNO_3 is the sum of gas-phase and condensed HNO_3 . The cirrus data set of 10-s averages is the same as the set of colored points in Fig. 1. The contrail data are shown for 13 July (red triangles) and 19 July (blue triangles). The use of the right-hand axis is discussed in the caption of Fig. 2. The diagonal dashed line represents the amount of total HNO_3 in the vapor phase on the NAT-ice coexistence phase boundary (39). Points above the line represent cloud parcels with sufficient HNO_3 and sufficiently low temperature that the NAT phase is stable. The points with NAT stability all correspond to data points below 202 K in Fig. 1, which have an average RH_i of 135%. This correspondence is the basis of the proposed NAT stability requirement for Δ -ice formation. As discussed in the text and shown in Fig. 2, NAT does not actually form in the bulk and control the HNO_3 vapor pressure. However, the cloud parcels with NAT stability also have the highest average surface coverages of HNO_3 , as shown by comparison with Fig. 1.



found to be condensed on essentially all of the ice particle samples reported here (Figs. 1 and 2), which is consistent with other observations in mid- and high-latitude low-temperature cirrus (25–27). Mass accommodation coefficients of up to 0.4 indicate that HNO_3 is readily adsorbed onto the low-temperature surfaces of liquid water and ice (28–33). On board the aircraft, HNO_3 was measured in situ with two independent detection channels (16): one channel for gas-phase HNO_3 and the other for gas-phase and condensed-phase HNO_3 . By combining HNO_3 and particle size and number measurements, the amount of condensed-phase HNO_3 per unit of particle surface area was calculated. Condensed HNO_3 amounts are expressed in units of molecules cm^{-2} (see color bar in Fig. 1) or as monolayers of ice-particle surface coverage, assuming that a monolayer is equal to approximately 10^{15} molecules cm^{-2} (Fig. 2). Average coverage as a function of temperature shows an increase with decreasing temperature, especially below 200 K (Fig. 1). For most of the data, measured total amounts of HNO_3 could provide coverages of between 0.1 and several monolayers (Fig. 2). However, observed condensed HNO_3 amounts are equivalent to 0.1 monolayer coverage or less.

Although our observations show HNO_3 uptake by ice particles, the thermodynamic state of this condensed HNO_3 is not known. Laboratory studies indicate that HNO_3 is strongly bound on the ice surface and has low bulk solubility (34–36). Furthermore, it is expected that HNO_3 in bulk ice readily diffuses to the ice surface (37). The supercooled HNO_3 - H_2O binary solution, nitric acid trihydrate ($HNO_3 \cdot 3H_2O$ or NAT), and ice are the only thermodynamically stable condensed phases for the range of total HNO_3 and H_2O values associated with the data in Fig. 1 (16). NAT stability as a function of temperature and the HNO_3/H_2O abundance ratio is based on laboratory measurements (39, 40). As shown in Fig. 3, only sampled cloud parcels with temperatures lower than approximately 200 K have conditions suitable for NAT formation. It is the same small fraction of parcels that has an average RH_i of 135% in Fig. 1. The lowest-temperature contrail data (13 July) also fall in the stability region, whereas the contrail data showing threshold behavior (19 July) fall just outside. Thus, a requirement for NAT stability is largely consistent with the observations of enhanced average RH_i below 202 K.

We propose that HNO_3 molecules adsorbed on cirrus cloud particles under NAT stability conditions combine with surface H_2O molecules to form NAT or NAT-like molecules that interfere with the uptake of water molecules on the ice surface more than with evaporation. Such an ice particle is designated hereafter as a Δ -ice particle. For

Δ -ice, the uptake interference can be expressed as a reduction in the water condensation coefficient α that causes an increase in RH_i in a metastable equilibrium state according to the schematic in Fig. 4 (41). This schematic contrasts the flux balances over pure ice and Δ -ice. The condensation coefficient relates the overall collisional flux (Q_c) onto the various facets of an ice particle with the total evaporative flux (Q_e) from those facets (42). The coefficient accounts for the adsorbed molecules that evaporate before being incorporated into the crystal lattice. Based on the RH_i data presented here, the ratio $\alpha_{ice}/\alpha_{\Delta-ice}$ is approximately 1.3.

The general concept of Δ -ice is supported by theoretical and experimental studies that have addressed the role of impurities and microphysical processes in crystal growth and habit (43–46). Impurity molecules adsorbed individually, as two-dimensional layers, or as surface microclusters can lead to macroscopic effects such as changes in growth rate, supersaturation, or crystal habit. Laboratory experiments have shown that the presence of HNO_3 during ice crystal growth changes the crystal habit (47), that ethanol substantially slows the ice crystal growth rate (46), and that the accommodation coefficient of water vapor is reduced on ice surfaces doped with HCl or HBr (48). Changes of habit and growth rate provide strong evidence for a reduction in α at the growth sites of a complex crystal.

Specific support for the Δ -ice mechanism comes from the microphysical role of anti-freeze proteins (AFPs) in lowering the freezing point of liquid water in biological organisms (49). AFPs alter the equilibrium at the ice/water interface by bonding to crystal growth sites and inhibiting the further incorporation of water molecules into the crystal lattice (50, 51). The inhibition is a noncolligative process that lowers the freezing point of water by up to 2 K depending on the AFP and its concentration. Several mechanisms have been proposed to explain the effect of AFPs. One mechanism that has received substantial support is that, by occupying key growth sites, AFP molecules force a reduction in the radius of curvature of new growth (51). This change causes a reduction in freezing point (or an increase in vapor pressure in an ice/vapor system) as a result of the Kelvin effect.

NAT on the Δ -ice surface might reduce α in one or more ways ($\alpha_{\Delta-ice} < \alpha_{ice}$ in Fig. 4). First, NAT or NAT-like molecules could play a role similar to that of AFPs. Single molecules or clusters of molecules would preferentially form at growth sites (i.e., steps or other dislocations) on the ice surface. Because ice grows through step propagation (52) and at crystal discontinuities (53), these adsorbed molecules would reduce α but not reduce the evaporative flux that occurs at all

sites. Second, the formation of regions or partial layers of NAT could also reduce α . Based on laboratory studies, water molecules evaporate and readily leave a NAT layer as if it were an ice surface ($Q_{c,\Delta-ice} \approx Q_{e,ice}$ in Fig. 4) (54, 55). When they do, the structure of the layer is probably not altered, because an H_2O molecule from the ice substrate immediately below the layer can reform any severed HNO_3 - H_2O bonds. However, the reverse process, that of water molecules being taken up by the layer, is hindered at the surface of a NAT layer (56, 31). Furthermore, laboratory studies show that ice does not readily nucleate on the surface of bulk NAT (57) and so may not nucleate on these partial layers. For both ways noted here, the coverage fraction of NAT on the ice particle surfaces could be comparable to or lower than the increase in RH_i above 100%. The coverage would be lower if NAT selectively interferes at crystal growth sites, which are generally a small fraction of surface sites. In the present study, the fractional changes are comparable because α is changed by 1.3 for estimated HNO_3 coverages near 0.1 monolayer, which correspond to larger NAT coverages (~ 0.3

monolayer). Because of the uncertainty in estimating effective surface coverage for complex crystals, the estimated HNO_3 coverages are likely upper limits.

The HNO_3 vapor pressures observed over Δ -ice particles as implied in Fig. 2 are higher than the equilibrium NAT values, indicating that the NAT bulk phase is not controlling the HNO_3 vapor pressure. Without bulk NAT, the equilibrium HNO_3 partitioning between the gas and condensed phases is proportional to surface area as

$$[HNO_3]_c/[HNO_3]_g \sim [\alpha_{HNO_3} v/4k_d]SAD \quad (1)$$

where $[HNO_3]_c$ and $[HNO_3]_g$ are condensed and gas-phase HNO_3 concentrations, respectively; v is the HNO_3 molecular velocity; α_{HNO_3} is the surface mass accommodation coefficient on ice; and k_d is the HNO_3 desorption rate from the condensed phase. In the sampled natural cirrus clouds as shown in Fig. 2, $[HNO_3]_c/[HNO_3]_g$ in general is much less than unity, and $[HNO_3]_c$ is nominally proportional to SAD, consistent with Eq. 1. Because $[HNO_3]_c/[HNO_3]_g$ is constant for a given SAD, uptake that increases the cover-

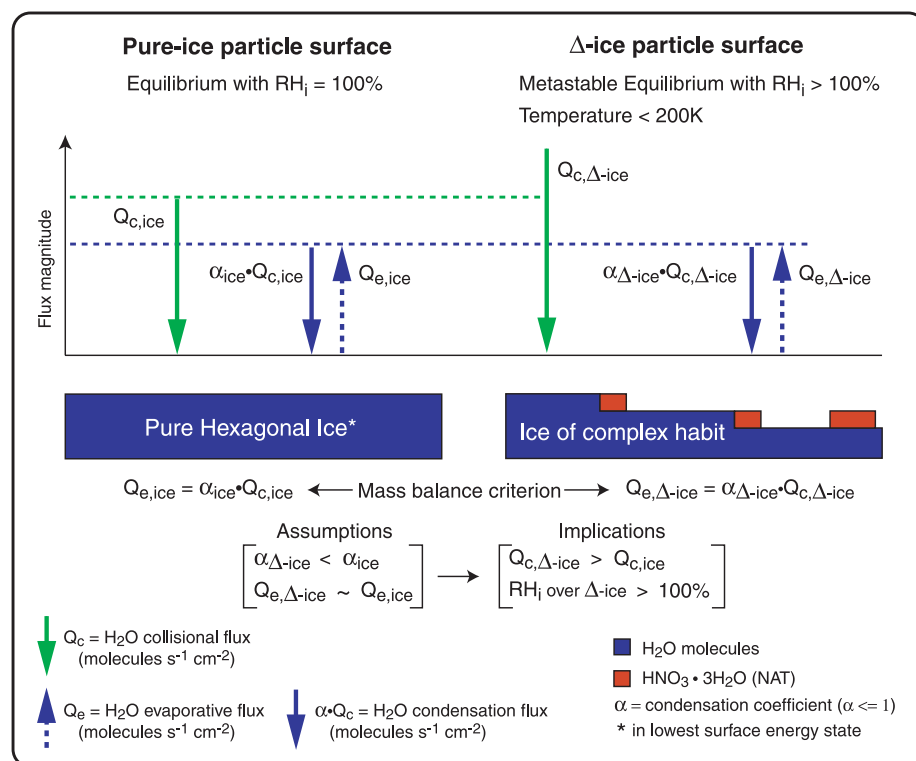


Fig. 4. Notional schematic of the fluxes at the surfaces of pure ice and Δ -ice particles and the metastable equilibrium mechanism of RH_i enhancement over the Δ -ice surface. Δ -ice particles are represented as having a complex habit (19) and having NAT (red blocks) present at various growth sites or as a partial layer. The green arrows represent the H_2O collisional flux at the ice surfaces. The blue arrows signify H_2O condensation (αQ_c) and evaporative (Q_e) fluxes, which for equilibrium conditions must satisfy the criterion of mass balance defined as $Q_e = \alpha Q_c$ (42). Two assumptions of the Δ -ice metastable equilibrium mechanism are (i) that the NAT present on Δ -ice reduces $\alpha_{\Delta-ice}$ below that of α_{ice} , and (ii) that the evaporation of water is not significantly impeded by the presence of NAT ($Q_{e,\Delta-ice} \approx Q_{e,ice}$). To balance the condensation and evaporation fluxes over Δ -ice, $Q_{c,\Delta-ice}$ must be larger than $Q_{c,ice}$, and therefore RH_i must be greater than 100%.

age of adsorbed HNO_3 in a Δ -ice population will be limited thermodynamically. This limit in turn bounds and stabilizes the RH_i enhancement in the population.

Confirming the existence of Δ -ice as a new particle class in the upper troposphere will require focused laboratory studies to complete the description of the microphysics of low-temperature ice with adsorbed HNO_3 . The present observations highlight the need to evaluate the potential role that other adsorbed impurities, such as organic molecules, might play in altering RH_i . For example, evidence from single-particle analysis shows that organic compounds are present on nearly all background aerosol particles in the mid- to upper troposphere (58).

The observations of enhanced and highly variable RH_i in low-temperature cirrus clouds as reported here have important implications for our understanding of the role of cloud microphysics in the radiative forcing of climate change. If assumed to be dependent primarily on temperature, enhanced RH_i should be present in natural and contrail clouds formed over a large fraction of the globe and over a significant altitude range. An increase in RH_i of 35% below 202 K as shown in Fig. 1 has an effect on water vapor that is equivalent to increasing cloud temperatures by 2 K. Thus, simulating these enhanced RH_i observations with cloud and climate models will result in reduced cloudiness and increased water vapor in the models in some upper tropospheric regions. These changes in turn will affect calculations of outgoing long-wave radiation at the top of the atmosphere (18) and the dehydration of air transported to the lower stratosphere.

The Δ -ice concept represents a direct link between climate change and natural and anthropogenic sources of HNO_3 . Produced indirectly from lightning and fossil fuel burning and transported directly from the stratosphere, HNO_3 is ubiquitous in the upper troposphere. HNO_3 abundances of hundreds of pptv are common (59–62), as are climatological temperatures below 202 K at low and high latitudes (63). Based on our proposed requirement of NAT stability, the formation of Δ -ice and the transition to higher RH_i will occur at different temperatures, depending on the ambient HNO_3 concentration. Near 200 K, increasing HNO_3 by 26% increases the NAT stability temperature by 1 K. Because HNO_3 abundances in the upper troposphere are significantly higher in the Northern Hemisphere than in the Southern Hemisphere (64), the frequency and extent of Δ -ice and its effect on climate parameters will likely be greater in the Northern Hemisphere. Finally, the formation of Δ -ice may be self-limiting, because HNO_3 (as well as water vapor) will be removed from the upper troposphere through Δ -ice particle sedimentation. Re-

moval of HNO_3 via adsorption on ice followed by sedimentation is an important component in the upper tropospheric budgets of reactive nitrogen (65, 66).

References and Notes

- D. Kley, J. M. Russell III, C. Phillips, Eds., *SPARC Assessment of Upper Tropospheric and Stratospheric Water Vapour*, (World Climate Research Programme No. 113, World Meteorological Organisation/TD No. 1043, SPARC Report No. 2, 2000).
- Climate Change, 2001: The Scientific Basis* [Intergovernmental Panel on Climate Change (IPCC), Cambridge Univ. Press, Cambridge, 2001].
- J. Tyndall, *Philos. Trans. R. Soc. London Ser. A* **A151**, 1 (1861).
- G. L. Stephens, T. J. Greenwald, *J. Geophys. Res.* **96**, 15311 (1991).
- J. E. Harries, *Q. J. R. Meteorol. Soc.* **122**, 799 (1996).
- E. F. Danielsen, *Geophys. Res. Lett.* **9**, 605 (1982).
- M. B. Baker, *Science* **276**, 1072 (1997).
- G. L. Stephens, in *Cirrus*, D. K. Lynch et al., Eds, (Oxford Univ. Press, Oxford, 2002), chap. 20.
- Special Report on Aviation and the Global Atmosphere* (IPCC, Cambridge Univ. Press, Cambridge, 1997).
- A. J. Heymsfield, R. P. Lawson, G. W. Sachse, *Geophys. Res. Lett.* **25**, 1335 (1998).
- E. J. Jensen et al., *Geophys. Res. Lett.* **25**, 1371 (1998).
- R. S. Gao et al., in preparation.
- A. Tabazadeh, O. B. Toon, *Geophys. Res. Lett.* **25**, 1379 (1998).
- A. Nenes et al., *Geophys. Res. Lett.* **29**, 10.1029/2002GL015295 (2002).
- Y. S. Djikaev, A. Tabazadeh, H. Reiss, *J. Chem. Phys.* **118**, 6572 (2003).
- Materials and methods are available as supporting material on Science Online.
- A. J. Heymsfield, L. M. Miloshevich, *J. Atmos. Sci.* **52**, 4302 (1995).
- E. J. Jensen et al., *J. Geophys. Res.* **106**, 17253 (2001).
- H. Vömel et al., *J. Geophys. Res.* **107**, 10.1029/2001JD000707 (2002).
- J. Ovarlez et al., *Geophys. Res. Lett.* **29**, 10.1029/2001GL014440 (2002).
- V. I. Khvorostyanov, K. Sassen, *J. Atmos. Sci.* **55**, 1822 (1998).
- Atmospheric wave activity is of interest because it can cause rapid and large temperature oscillations in upper tropospheric clouds and contrails. The supersaturation caused in a wave will be greater than the subsaturation because of the nonlinear dependence of RH_i on the water vapor pressure and the nonlinearity in the Clausius-Clapeyron equation relating vapor pressure and temperature. The increase in saturation in a cloud parcel in response to a temperature modulation has been evaluated as a function of temperature, ice particle size, and ice particle number density (27). The increases are small (5% or less) for the cloud and contrail conditions associated with the data in Fig. 1. Similarly, radiative heating rates are not expected to be important for the analysis of contrail cloud parcels reported here (28).
- Th. Peter et al., in preparation.
- E. J. Jensen, A. S. Ackerman, D. E. Stevens, O. B. Toon, P. Minnis, *J. Geophys. Res.* **103**, 31557 (1998).
- A. J. Weinheimer et al., *Geophys. Res. Lett.* **25**, 1725 (1998).
- S. Meilinger et al., *Geophys. Res. Lett.* **26**, 2207 (1999).
- Y. Kondo et al., *Geophys. Res. Lett.* **30**, 10.1029/2002GL016539 (2003).
- M.-T. Leu, *Geophys. Res. Lett.* **15**, 17 (1988).
- D. R. Hanson, *Geophys. Res. Lett.* **19**, 2063 (1992).
- P. K. Hudson, J. E. Shilling, M. A. Tolbert, O. B. Toon, *J. Phys. Chem. A* **100**, 9874 (2002).
- Chemical Kinetics and Photochemical Data for Use in Atmospheric Studies, Evaluation Number 14* (JPL Publication 02-25, NASA Jet Propulsion Laboratory, Pasadena, CA, 2003).
- M. A. Zondlo, S. B. Barone, M. A. Tolbert, *Geophys. Res. Lett.* **24**, 1391 (1997).
- O. P. Arora, D. J. Cziczo, A. M. Morgan, J. P. D. Abbatt, R. F. Niedziela, *Geophys. Res. Lett.* **26**, 3621 (1999).
- D. R. Hanson, A. R. Ravishankara, *J. Geophys. Res.* **96**, 5081 (1991).
- J. P. D. Abbatt, *Geophys. Res. Lett.* **24**, 1479 (1997).
- R. A. Sommerfeld, C. A. Knight, S. K. Laird, *Geophys. Res. Lett.* **25**, 935 (1998).
- F. Dominé, E. Thibert, *Geophys. Res. Lett.* **23**, 3627 (1996). However, we note that an older study (38) concluded that the diffusion of HNO_3 in ice is extremely slow.
- J. V. Iribarne, T. Pyshnov, *Atmos. Environ.* **24A**, 383 (1990).
- D. R. Hanson, K. Mauersberger, *Geophys. Res. Lett.* **15**, 855 (1988).
- D. R. Worsnop, L. E. Fox, M. S. Zahniser, S. C. Wofsy, *Science* **259**, 71 (1993).
- For simplicity, only an ice/vapor equilibrium is shown in Fig. 4 to illustrate the effect of Δ -ice on RH_i . In reality, both natural and contrail cirrus clouds are complex dynamic systems. Numerous measurements inside cirrus clouds (20, 21, 23), including this study, show large RH_i variabilities, indicating that the ice/vapor interaction consistently does not reach an equilibrium state defined by RH_i of 100%. Because $\alpha_{\Delta\text{-ice}}$ is less than α_{ice} , RH_i will be affected by Δ -ice even though the ice/vapor system is not in equilibrium.
- J.-P. Chen, D. Lamb, *J. Atmos. Sci.* **51**, 1206 (1994).
- J. T. Nelson, M. B. Baker, *J. Geophys. Res.* **101**, 7033 (1996).
- K. Sangwal, *Prog. Cryst. Growth Charact.* **32**, 3 (1996).
- V. S. Veintimillas-Verdaguer, *Prog. Cryst. Growth Charact.* **32**, 75 (1996).
- J. Neustaedter, I. Gallily, *J. Cryst. Growth* **85**, 422 (1987).
- V. J. Schaefer, *Chem. Rev.* **44**, 291 (1949).
- C. Delval, B. Fluckiger, M. J. Rossi, *Atmos. Chem. Phys.* **3**, 1131 (2003).
- A. L. DeVries, D. E. Wohlshlag, *Science* **163**, 1073 (1969).
- J. A. Raymond, A. L. DeVries, *Proc. Natl. Acad. Sci. U.S.A.* **74**, 2589 (1977).
- Y. Yeh, R. E. Feeney, *Chem. Rev.* **96**, 601 (1996).
- K. C. Young, *Microphysical Processes in Clouds* (Oxford Univ. Press, Oxford, 1993).
- S. E. Wood, M. B. Baker, D. Calhoun, *J. Geophys. Res.* **106**, 4845 (2001).
- U. M. Biermann et al., *Geophys. Res. Lett.* **25**, 3939 (1998).
- M. S. Warshawsky, M. A. Zondlo, M. A. Tolbert, *Geophys. Res. Lett.* **26**, 823 (1999).
- A. M. Middlebrook, B. G. Koehler, L. S. McNeil, M. A. Tolbert, *Geophys. Res. Lett.* **19**, 2417 (1992).
- S. B. Barone, M. A. Zondlo, M. A. Tolbert, *J. Phys. Chem. A* **101**, 8643 (1997).
- D. M. Murphy, D. S. Thomson, M. J. Mohoney, *Science* **282**, 1664 (1998).
- R. W. Talbot et al., *J. Geophys. Res.* **102**, 28303 (1997).
- L. Jaegle et al., *Geophys. Res. Lett.* **25**, 1705 (1998).
- R. W. Talbot et al., *Geophys. Res. Lett.* **26**, 3057 (1999).
- J. A. Neuman et al., *Atmos. Environ.* **35**, 5789 (2001).
- Reference upper tropospheric temperature data are from National Center for Environment Prediction (NCEP) reanalyzed temperature data averaged over 23 years. The known positive bias in NCEP temperatures of about 4 K is taken into account here.
- J. Baehr et al., *Geophys. Res. Lett.* **30**, 10.1029/2003GL016935 (2003).
- M. G. Lawrence, P. J. Crutzen, *Tellus* **50B**, 263 (1998).
- A. Tabazadeh, O. B. Toon, E. J. Jensen, *Geophys. Res. Lett.* **26**, 2211 (1999).
- The authors appreciate discussions with J. P. D. Abbatt, M. B. Baker, D. R. Hanson, E. J. Jensen, C. A. Knight, N. Lovejoy, D. M. Murphy, L. Pfister, A. R. Ravishankara, A. F. Tuck, A. S. Wexler, and S. E. Wood. We thank the pilots, sensor operators, and ground crew of the NASA WB-57F aircraft. This work was partially supported by the Upper Atmospheric Research Program and the Radiation Science Program of NASA.

Supporting Online Material
www.sciencemag.org/cgi/content/full/303/5657/516/DC1
 Materials and Methods
 Fig. S1
 Table S1
 References

8 September 2003; accepted 17 December 2003